Science Signaling
AAAS

www.sciencesignaling.org/cgi/content/full/5/213/ra17/DC1

Supplementary Materials for

Diverse Sensitivity Thresholds in Dynamic Signaling Responses by Social Amoebae

C. Joanne Wang, Adriel Bergmann, Benjamin Lin, Kyuri Kim, Andre Levchenko*

*To whom correspondence should be addressed. E-mail: alev@jhu.edu

Published 28 February 2012, *Sci. Signal.* **5**, ra17 (2012)
DOI: 10.1126/scisignal.2002449

This PDF file includes:

Other Supplementary Material for this manuscript includes the following:
(available at www.sciencesignaling.org/cgi/content/full/5/213/ra17/DC1)

Movies S1 to S14 (.avi format). Translocation kinetics of PHcrac-GFP in cells stimulated under various conditions.

Text S1: Determining the threshold for partitioning responders from non-responders.

The partitioning threshold used to distinguish responders from non-responders was chosen as follows. The observed response frequency distribution for all cAMP doses used in the experiments was fitted twice, first to a single Gaussian and then to two Gaussian distributions (Fig. T1). The ratio of the reduced Chi-squared values, correcting for the reduction in the degrees of freedom for the two Gaussians fit, are shown in the figures. The quality of the fits improved substantially when two, rather than a single Gaussian distribution were used for fitting, supporting the existence of two distinct sets of responses. The intersection point of the two fitted Gaussians was then used to set the partition threshold.

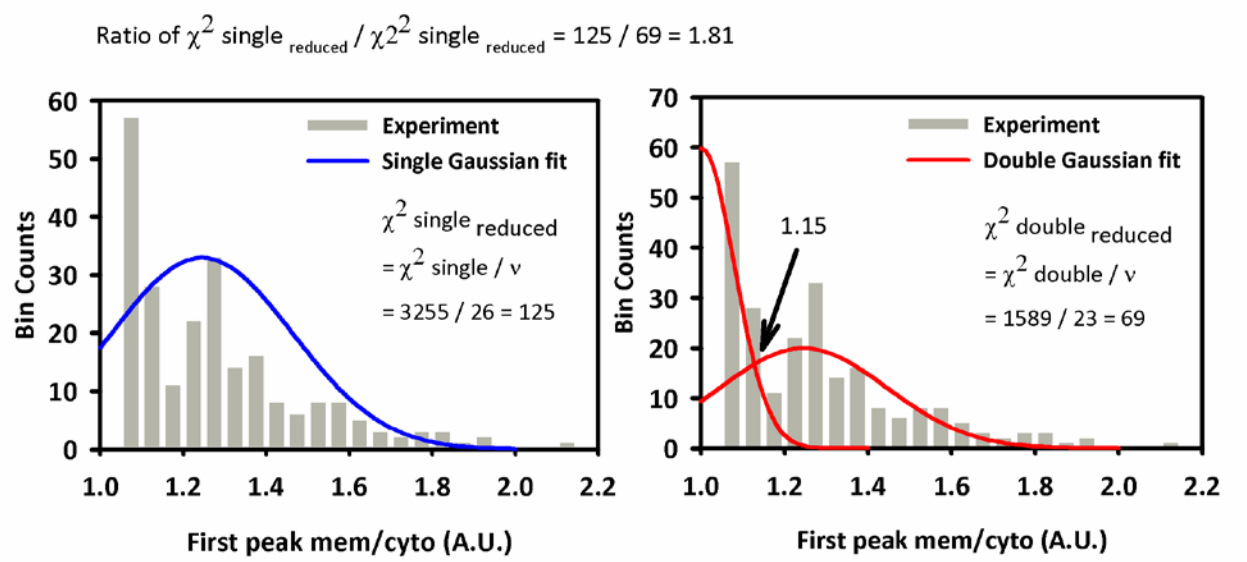

Fig. T1. The observed response frequency distribution for all cAMP doses used in the experiments was fitted twice, first to a single Gaussian and then to two Gaussian distributions. The intersection point, 1.15, is the threshold used to partition responders from non-responders.

Text S2. Comparing the responses of single integral feedback and feedforward loops to ramp input.

Both the incoherent feed-forward and integral feedback systems are capable of resetting to baseline in response to a single-step disturbance (*1*). The integral feedback control type circuits achieves perfect adaptation by continuously monitoring the difference between input and output, therefore a single circuit will fail to adapt to a linear ramp stimuli (Fig. T2) (*2*). Therefore, at least two integral feedback circuits coupled in sequence are required to achieve perfect adaptation to linear ramp stimuli, with the first converting the stimulus into a persistent output and the second circuit converting this persistent output into a transient response returning to the baseline (*2*). In comparison, only a single incoherent feed-forward circuit is required to adapt to a linear ramp, because it determines the degree of resetting by directly monitoring the input (Fig. T2). The adaptation responses we measured when cells are exposed to cAMP suggest either a single incoherent feed-forward circuit (such as LEGI) is present, or alternatively, at least two sequential integral feedback circuits. Due to its relative simplicity, we have continued using the feedforward scheme in the aLEGI model throughout the study.

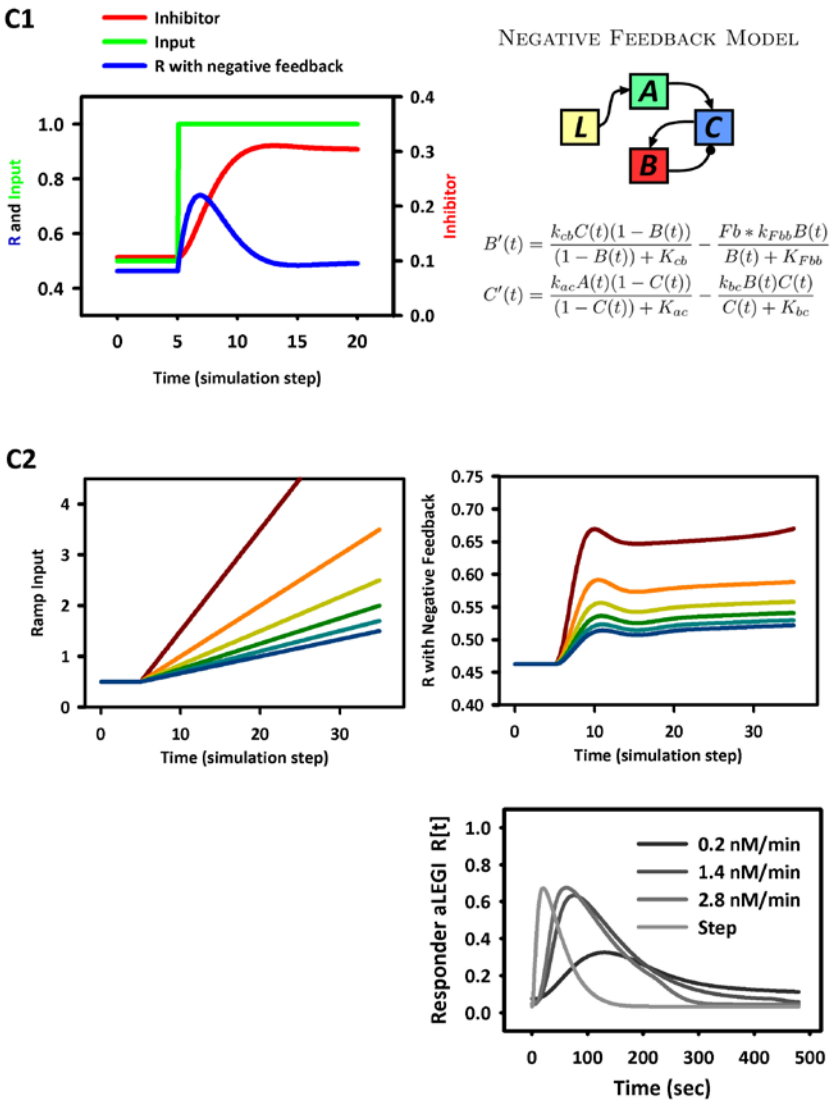

Fig. T2. Integral feedback response to a ramp stimulation. Two possible three-node network motifs for perfect adaptation were considered: Integral negative feedback and incoherent feedforward loop. Both network topologies are capable of resetting to baseline in response to a single-step disturbance. **C1**. Integral control feedback circuit response to step input. A directly mirrors the input (L) concentration, B is the negative inhibitor, and C is the negative feedback response element. The following parameter values were used in the Mathematica simulation: K_{cb} = 0.01, K_{Fbb} = 0.01, k_{cb} = 0.2, F_b = 1.0, k_{Fbb} = 0.1, k_{ac} = 1.0, K_{ac} = 1.0, k_{bc} = 2.0, K_{bc} = 0.1. **C2**. Integral control type circuits achieves perfect adaptation by continuously monitoring the difference between input and the output, therefore single integral feedback loop fails to adapt to a linearly increasing stimuli (upper left and right panels). This result is robust against parameter variation. The feedforward adaptation circuit can adapt to a linear ramp because it determines the degree of resetting by directly monitoring the input. Lower right panels: the result of aLEGI originally presented in Fig. 4C is reproduced here for the convenience of comparison.

Text S3: Method for gradient sensing analysis.

The main drawback of the LEGI module as a stand-alone model is its failure to generate the experimentally observed switch-like polarization response in the gradient of the intraceullar signaling. Mechanisms such as the "balanced inactivation" scheme have been proposed as a potential modification of the LEGI model to address this shortcoming (*3*). However, the balanced inactivation model has the essential drawback of being unable to explain the apparently absent response in absence of complete resetting of the sensitivity of the pathway (for example, the refractory period observed in this study). As shown in the main text, the aLEGI model can also allow for a strong amplification of the response gradient. The LEGI module transforms the extracellular gradients of cAMP into a gradient of LEGI responses, the slope of which mirrors the external gradient closely if the inhibitor's diffusion coefficient is sufficiently high. However, in the context of the aLEGI model, the amplifier module can convert the more graded input from LEGI to a more switch-like response, in a manner dependent on the θ values of the individual cells (Fig. 5A).

The gain of the intracellular gradient amplification for various extracellular gradient and θ values was estimated using the following metric:

$$Gain_{\theta,gradient} = \frac{Front\ amplitudes\ of\ the\ aLEGI\ response - Back\ amplitudes\ of\ the\ aLEGI\ response}{Extracellular\ Gradient\ Value}$$

Text S4: Setup and development of the collective cell response model.

Below we list the assumptions underlying the simple model of collective cell responses. We note that although are model is conceptually similar to a study by Vasieva *et al*. (*4*), the details are sufficiently different to qualify the present model as completely distinct. The assumptions are consistent with the aLEGI model properties, including the differential sensitivity to both spatially homogeneous and spatially graded cAMP inputs across the cell population, as discussed in the main text.

1) An N x N simulation grid is used with K cells seeded on it, one of which is selected as the pulsing source of the cAMP signal with a period P;
2) Each cell is in one of three states: Unstimulated, Responding, or Recovering in sensitivity (based on the cell memory discussed in the main text);
3) Cell-cell communication is characterized by the spatial signaling radius is R, that is a resting cell within a radius of R from a Responding cell (assumed to be secreting the cAMP signal; cAMP secretion is equal for all Responding cells) can becomes itself Responding at the next time step, and then move by a displacement distance S in the direction of maximum input concentration. Once excited, cells stay in the Recovering mode for a period of F time steps, defined by the cell memory. As specified below,

whether a cell responds or not depends on its response threshold (per aLEGI model), expressed in terms of different effective spatial signaling radius.

In this model implementation, we simplified the analysis by simulation of a dual threshold response by assigning each cell in the population one of two effective spatial signaling radius values, R_1 or R_2. For instance, the cells with a lower threshold for responding to cAMP will have the larger value R_2. We implemented this simple multicellular model in Mathematica (Wolfram) with the following parameters: N = 300; K = 1089; P = 6; F = 3; S = 5. The R values used are specified in the figures. We used this modified model to study the temporal progression of the spatial patterns of the reorganizing cell population as a function of the heterogeneity of the population.

Fig. 6A of the main text shows the examples of heterogeneous and homogeneous populations, and illustrates different temporal evolutions for these two population types. The effective spatial signaling radius (R_{eff}) used in Fig. 6 is defined as follows:

$$R_{eff} = f_1 R_1 + (1-f_1)R_2,$$

where f_1 is the fraction of the population that has the higher threshold, and R_1 and R_2 are defined above. f_1 was allowed to vary from 0 to 1, 1 corresponding to a homogeneous population with a high threshold, 0 to a homogeneous population with a low threshold. In Fig. 6A, the heterogeneous population was constructed to have an identical effective spatial signaling radii as that of the homogeneous population ($R_{homog} = R_{eff}$). The behaviors of these two populations are then quantified in Fig. 6B, by plotting the asymptotic time against the effective spatial signaling radius, where the asymptotic time is defined to be the time at which 90% of the cells have stopped streaming towards the pulsing source. The results suggest that, even though the heterogeneous and homogeneous populations have the same average effective spatial signaling radius values, the heterogeneous population converges more rapidly to a defined pattern compared to the homogeneous one.

Text S5: Mathematical description of the aLEGI model.

The Amplified LEGI Model

1 Equations

$$a'(t) = \rho_a(k_l * L - k_d * a(t) + k_c) \tag{1}$$
$$i'(t) = \rho_i(k_l * L - k_d * i(t) + k_c) \tag{2}$$
$$r'(t) = \rho_r(a(t) * (r_{tot} - r(t)) - i(t) * r(t)) \tag{3}$$
$$amp'_\theta(t) = \rho_m \left(\frac{r(t) * (amp_{tot} - amp_\theta(t))}{K_m + (amp_{tot} - amp_\theta(t))} - \frac{\theta * amp_\theta(t)}{K_m + amp_\theta(t)} \right) \tag{4}$$

2 Initial Conditions

$$a(0) = k_c/k_d \qquad = 0.05 \text{ nM} \tag{5}$$
$$i(0) = k_c/k_d \qquad = 0.05 \text{ nM} \tag{6}$$
$$r(0) = r_{tot} * \frac{a(0)}{a(0) + i(0)} \qquad = 0.5 \text{ nM} \tag{7}$$

$\text{amp}_\theta(0)$ is the pre-equilibration output of the model at zero stimulus

3 Parameters

L	$[10^{-3} - 10^4]$ nM	Input cAMP concentration
k_l	0.3	Induced activation rate for a and i
k_d	2.0	Inactivation rate for a and i
k_c	0.1 nM	Constitutive activation rate for a and i
ρ_a	0.1 sec^{-1}	Rate of excitor dynamics
ρ_i	0.01 sec^{-1}	Rate of inhibitor dynamics
ρ_r	1.0 sec^{-1}	Rate of LEGI response dynamics
ρ_m	0.3 sec^{-1}	Rate of amplified response dynamics
K_m	0.01 nM	Saturation constant
θ	U[0.55 - 0.9] nM	Threshold for amplified response
r_{tot}	1.0 nM	Total amount of LEGI response
amp_{tot}	1.0 nM	Total amount of amplified response

Supp. Figure 1

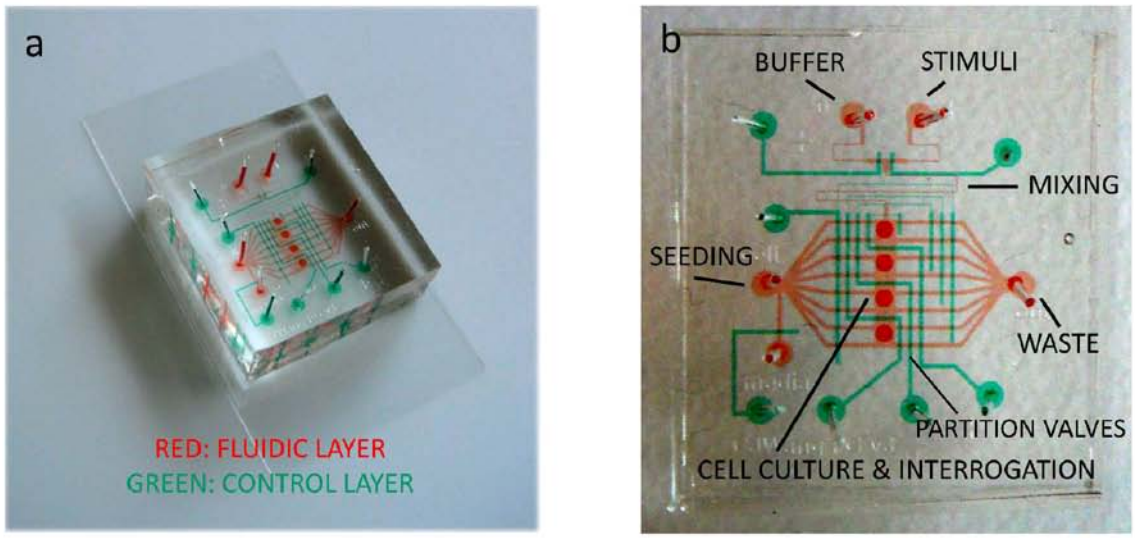

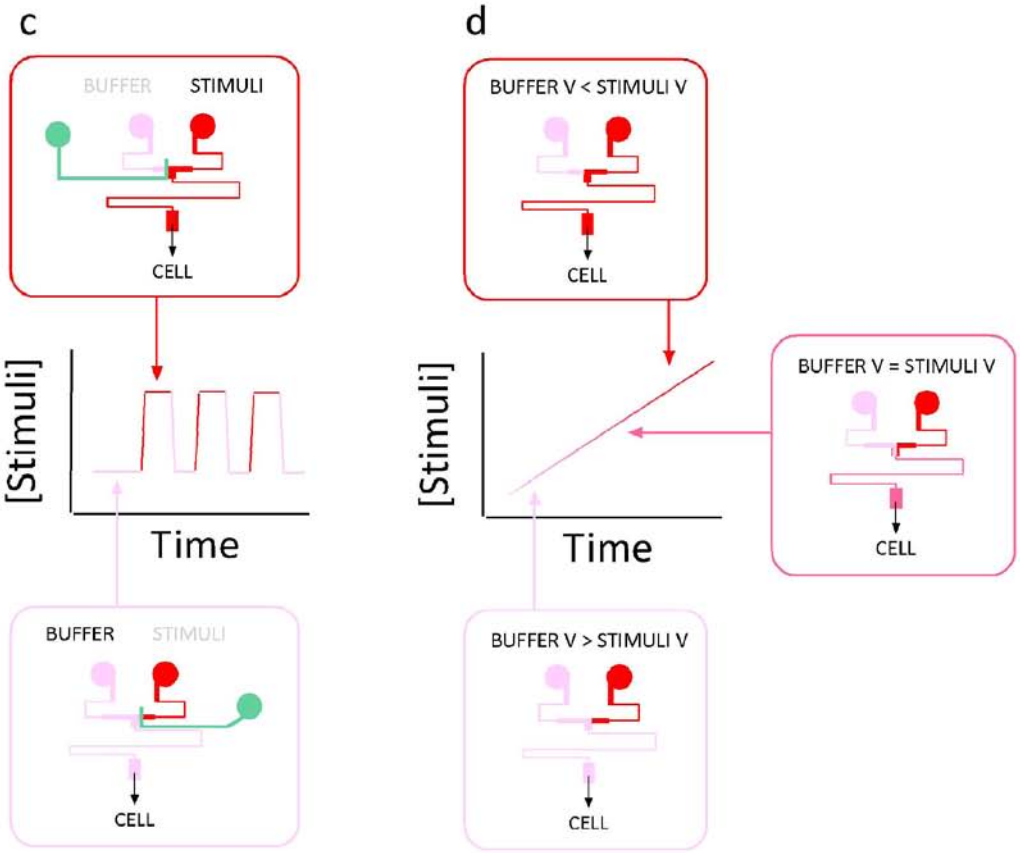

Figure S1. The microfluidic function generator.

a. A photograph of the device and **b**. design layout. The custom microfabricated PDMS device was bonded to a glass coverslip and filled with food dyes to facilitate visualization. The chip contained two layers. The bottom layer (visualized with red food dye) contained a cell culture chamber connected by a mixing channel to the two signal inlets, and a separate set of channels for waste output and cell introduction. Two upper control channels (visualized with green food dye) controlled stimuli entry and exit, the remaining partitions the cell culture chamber into multiple compartments, allowing independent experimentation in subsets of the chamber.

c. Stimulation profile of oscillatory square waveform with arbitrary periods and duty cycles was generated by selectively actuating the valves gating the inlets containing the washing buffer and the stimuli.

d. Arbitrary stimuli concentration profiles were produced by mixing the washing buffer and the stimuli flowing at different relative volumetric flow rates (designated as V in the diagram). Ramp stimuli and pulsatile waves were generated based on similar principle, except the relative volumetric flow rate dynamically changed with respect to time instead of remaining fixed.

Supp. Figure 2

a

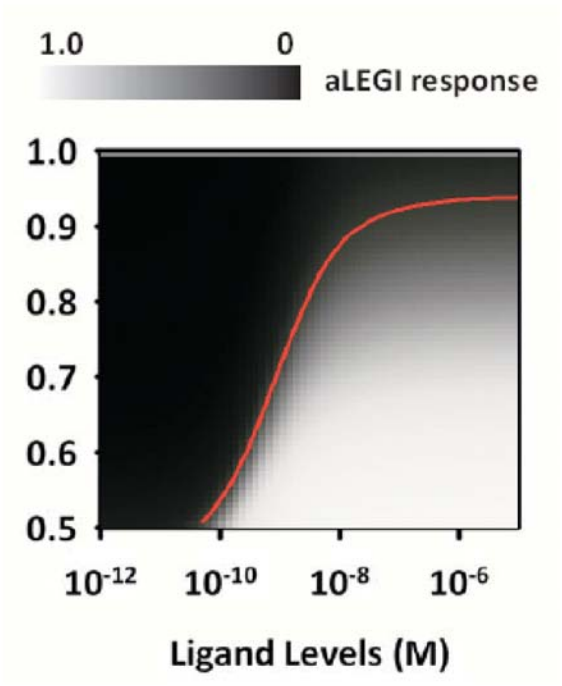

Supp. Figure 2

b

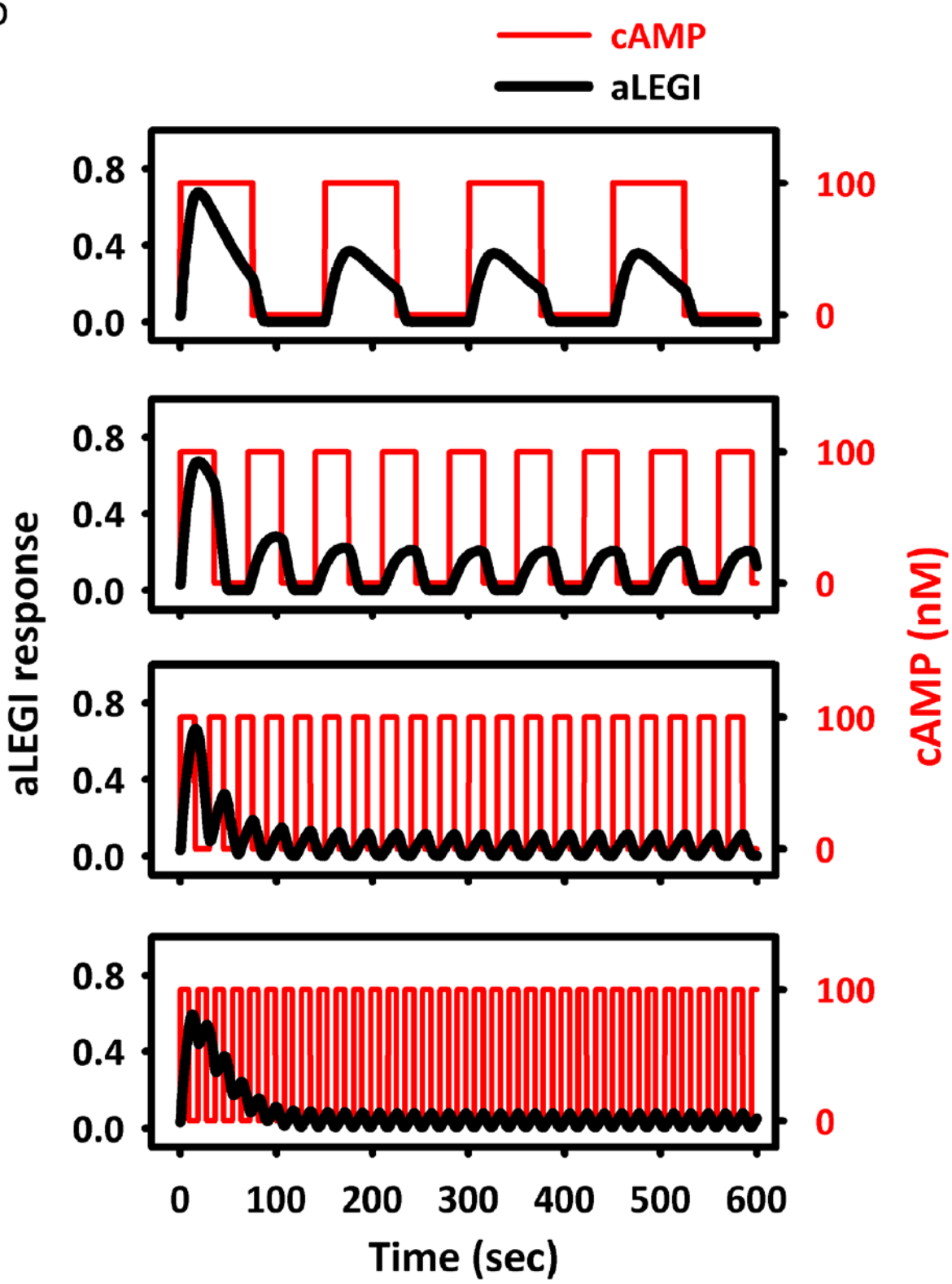

Figure S2. The properties of aLEGI model.

a. Simulated single cell dose response. Peak aLEGI responses to different combinations of threshold and ligand amounts plotted as a density plot. Red line: responder value.

b. Simulation of cells stimulated with square wave trains with periods of 140 s, 70 s, 30 s, 18 s (from top to bottom). The input profiles are shown in red, and the aLEGI responses in black.

Supp. Figure 3

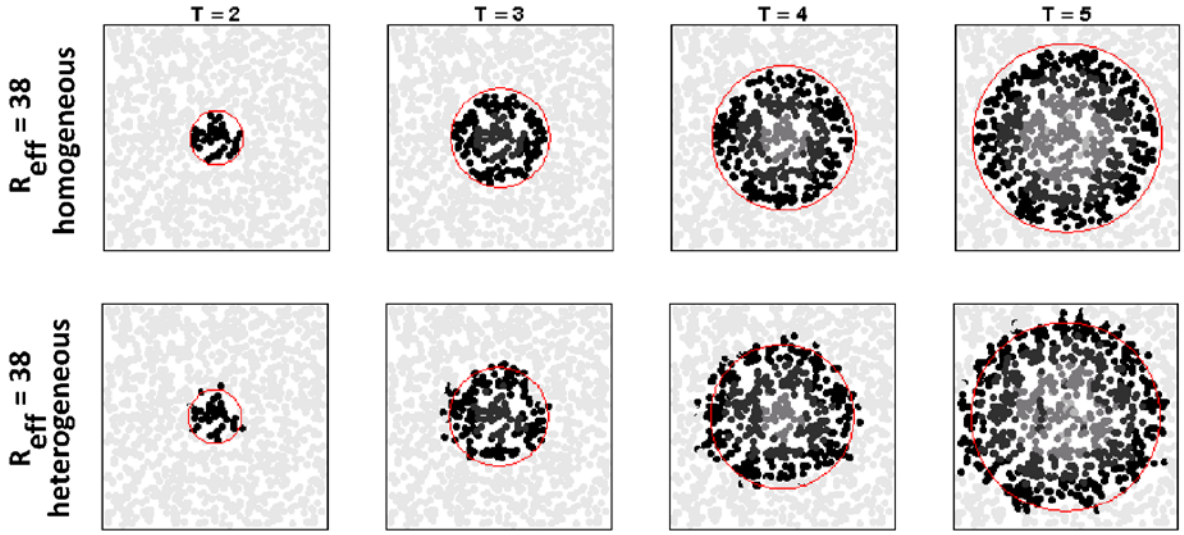

Figure S3. Schematic mechanism of increased rate of cAMP wave propagation as a function of the colony heterogeneity. The red circles were identical for each corresponding snapshot of the two populations. Cells outside of the red circle get excited because they have a larger sensing radius. This process repeats itself at every pulse, thus efficiently recruiting more cells that are farther away from the pulsing center.

Supp. Figure 4

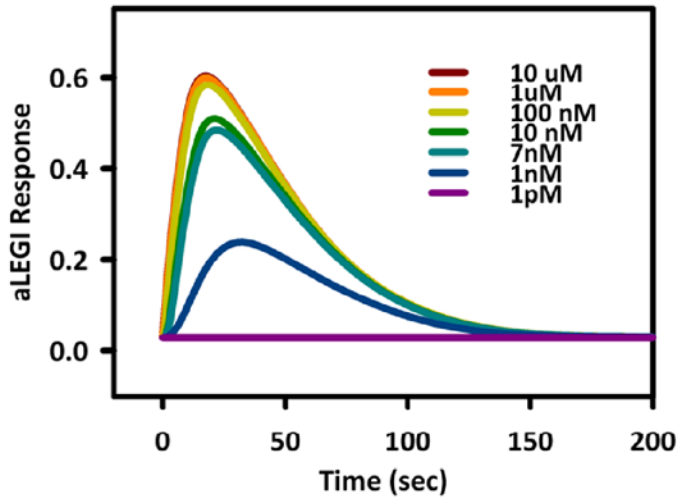

Figure S4. Simulation of the average dose response dynamics

Supp. Figure 5

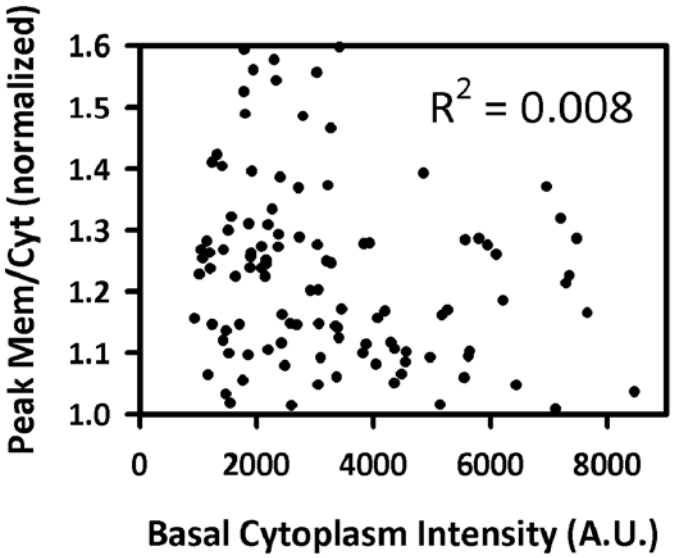

Figure S5. Dependence of PIP_3 responses on probe expression. Peak PIP_3 translocation responses to a step input of cAMP for doses 1 to 100 nM in a single cell compared to basal PHcrac-GFP expression. The scattered plot is fitted to a line and the R-square value is 0.008.

Supp. Figure 6

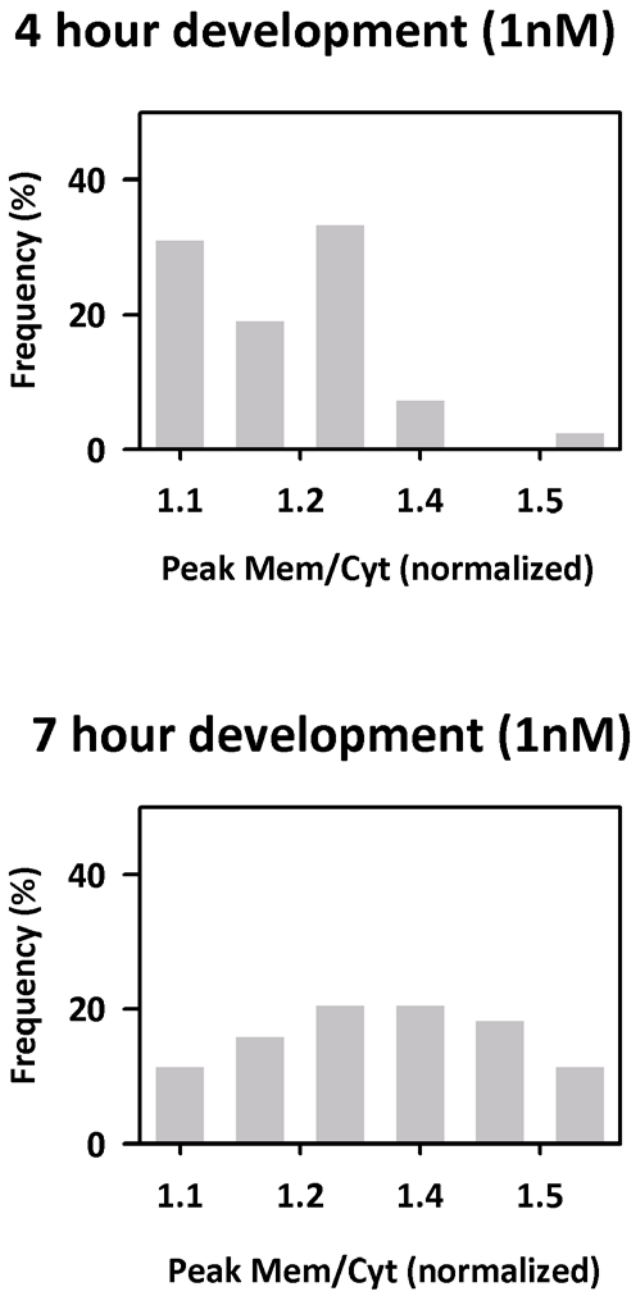

Figure S6. Distribution of cell responses to step stimulation at two different developmental stages. Top, Reproduction of Fig. 1C for comparison with the bottom figure. Bottom, histogram of the peak responses to a step input of 1nM cAMP after the cells were developed for 7 hours.

Supp. Figure 7

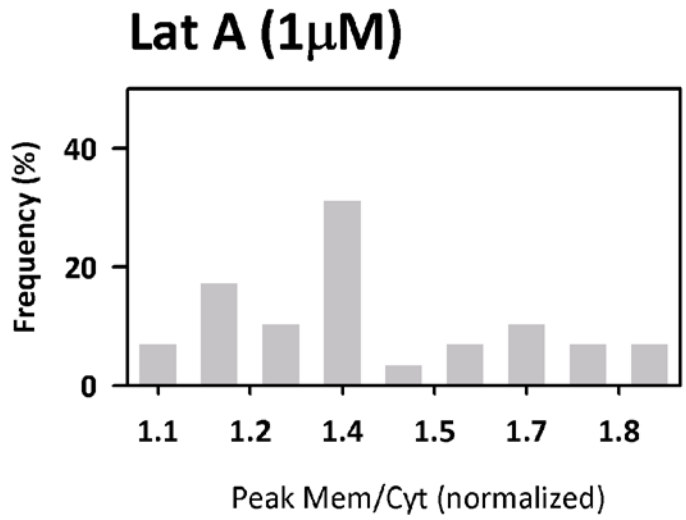

Figure S7. Responses after latrunculin A treatment. Histogram of the peak responses to a step input of 1 μM cAMP after the cells were developed for 4 hours then treated with latrunculin A (Lat-A) prior to stimulation.

References

1. W. Ma, A. Trusina, H. El-Samad, W. A. Lim, C. Tang, Defining Network Topologies that Can Achieve Biochemical Adaptation. *Cell* **138**, 760-773 (2009).
2. D. Muzzey, C. A. Gómez-Uribe, J. T. Mettetal, A. van Oudenaarden, A Systems-Level Analysis of Perfect Adaptation in Yeast Osmoregulation. *Cell* **138**, 160-171 (2009).
3. H. Levine*,* D. A. Kessler, W.J. Rappel*,* Directional Sensing in Eukaryotic Chemotaxis: A Balanced Inactivation Model. *Proc. Natl. Acad. Sci. USA* **103**, 9761-66 *(*2006).
4. O. O. Vasieva, B. N. Vasiev, V. A. Karpov, A. N. Zaikin, A model of Dictyostelium aggregation. *J. Theor*. *Biol*. **171**, 361–367 (1994).

Movie S1. Translocation kinetics of PHcrac-GFP in response to 10 nM cAMP.

Movie S2. Translocation kinetics of PHcrac-GFP in response to 1 nM cAMP.

Movie S3. Translocation kinetics of PHcrac-GFP in response to 1 pM cAMP, example 1.

Movie S4. Translocation kinetics of PHcrac-GFP in response to 1 pM cAMP, example 2.

Movie S5. Translocation kinetics of PHcrac-GFP in response to 1 pM cAMP stimulation for 5 min, then 1 μm cAMP for another 5 min.

Movie S6. Translocation kinetics of PHcrac-GFP in response to 100 nM cAMP stimulation for 5 min, washed with buffer for 20 s, re-stimulated with 100 nM cAMP for another 5 min.

Movie S7. Translocation kinetics of PHcrac-GFP in response to 100 nM cAMP stimulation for 5 min, washed with buffer for 1 min, re-stimulated with 100 nM cAMP for another 5 min.

Movie S8. Translocation kinetics of PHcrac-GFP in response to 100 nM cAMP stimulation for 5 min, washed with buffer for 2 min, re-stimulated with 100 nM cAMP for another 5 min.

Movie S9. Translocation kinetics of PHcrac-GFP in response to 100 nM cAMP stimulation for 5 min, washed with buffer for 4 min, re-stimulated with 100 nM cAMP for another 5 min.

Movie S10. Translocation kinetics of PHcrac-GFP in cells stimulated with pulse trains of 100 nM cAMP at 56 mHz.

Movie S11. Translocation kinetics of PHcrac-GFP in cells stimulated with pulse trains of 100 nM cAMP at 40 mHz.

Movie S12. Translocation kinetics of PHcrac-GFP in cells stimulated with pulse trains of 100 nM cAMP at 14 mHz.

Movie S13. Translocation kinetics of PHcrac-GFP in cells stimulated with pulse trains of 100 nM cAMP at 7 mHz.

Movie S14. Translocation kinetics of PHcrac-GFP in cells stimulated with 10 nM cAMP for 5 min, washed with buffer for 10 min, then stimulated with ramp stimuli of 0.2 nM/min.